Chapter 6

Performance Evaluation of Nanofluids in an Inclined Ribbed Microchannel for Electronic Cooling Applications

Mohammad Reza Safaei, Marjan Gooarzi, Omid Ali Akbari, Mostafa Safdari Shadloo and Mahidzal Dahari

Additional information is available at the end of the chapter

http://dx.doi.org/10.5772/62898

Abstract

Nanofluids are liquid/solid suspensions with higher thermal conductivity, compared to common working fluids. In recent years, the application of these fluids in electronic cooling systems seems prospective. In the present study, the laminar mixed convection heat transfer of different water–copper nanofluids through an inclined ribbed microchannel—as a common electronic cooling system in industry—was investigated numerically, using a finite volume method. The middle section of microchannel's right wall was ribbed, and at a higher temperature compared to entrance fluid. The modeling was carried out for Reynolds number of 50, Richardson numbers from 0.1 to 10, inclination angles ranging from 0° to 90°, and nanoparticles' volume fractions of 0.0–0.04. The influences of nanoparticle volume concentration, inclination angle, buoyancy and shear forces, and rib's shape on the hydraulics and thermal behavior of nanofluid flow were studied. The results were portrayed in terms of pressure, temperature, coefficient of friction, and Nusselt number profiles as well as streamlines and isotherm contours. The model validation was found to be in excellent accords with experimental and numerical results from other previous studies.

The results indicated that at low Reynolds' flows, the gravity has effects on the heat transfer and fluid phenomena considerably; similarly, with inclination angle and nanoparticle volume fraction, the heat transfer is enhanced by increasing the Richardson number, but resulting in a less value of friction coefficient. The results also represented that for specific Reynolds (Re) and Richardson (Ri) numbers, heat transfer and pressure drop augmented by increasing the inclination angle or volume fraction of nanoparticles. With regard to the coefficient of friction, its value decreased by adding less nanoparticles to the fluid or by increasing the inclination angle of the microchannel.

Keywords: mixed convection heat transfer, inclined ribbed microchannel, nanofluid, finite volume method, friction factor

1. Introduction

Electronics have turned smaller, quicker, and more powerful due to the current development in computing technology during the past few decades, resulting in a dramatic rise in the rate of heat generation from electronic appliances. One way to keep the heat generated by different parts of electronic devices within safety zone is to cool the chips via forced air flow. However, standard cooling procedures seem insufficient to deal with the parts which are comprised of billions of transistors functioning at high frequency, considering the fact that the temperature can rise up to a critical point. Thus, microscale cooling appliances like microchannel heat sinks have vital roles in heat removal applications in appliances including high-energy mirrors and laser diode arrays [1]. In 1981, Tuckerman and Pease brought up the concept of a microchannel heat exchanger first [2]. The major advantage of a microchannel heat sink is the fact that its heat transfer coefficient is much higher than the traditional heat exchangers [3]. This causes microchannels to become useful for being employed in semiconductor power devices, very large-scale integrated (VLSI) circuits, etc. [4]. The first idea was to utilize water as a coolant in microchannels as cooling systems [5, 6]. Nevertheless, water is subjected to weak thermophysical properties. The convective heat transfer rate of these types of working fluids can be enhanced by improving their thermophysical properties. Nanofluids prepared through dispersing nanosized particles into the base fluid for the sake of enhancing the thermophysical properties of the working fluid are considered to support higher heat transfer compared to conventional fluids, such as water [7], ethylene glycol [8], kerosene [9], etc.

Recently, heat transfer and nanofluid flow in microchannels have drawn enormous interests by researchers. However, most of the researches are concerned with the forced convection heat transfer in smooth microchannels. The laminar forced convection heat transfer of γ-Al_2O_3/deionized water nanofluid through a rectangular microchannel heat sink was studied by Kalteh et al. [10], using a finite volume method. Moreover, they carried out experimental study to make comparison between the outcomes with numerical results. Their findings demonstrated that average Nusselt number rises with a growth in Re and vol. % of nanofluid besides a reduction in the nanoparticle size.

The theoretical study of laminar forced convection heat transfer of Al_2O_3/H_2O nanofluid inside a circular microchannel accompanied by a uniform magnetic field was carried out by Malvandi and Ganji [11]. Due to the nonadherence of the fluid–solid interface accompanied by nanoparticle migration, considered as a slip condition, and also the microscopic roughness in circular microchannels, the Navier's slip boundary condition was applied to the walls. The results of this research showed that the near-wall velocity gradients rise by applying the magnetic field, improving the slip velocity, and therefore, the pressure drop and heat transfer rate rise.

http://dx.doi.org/10.5772/62898

The heat transfer and fluid flow of MWCNT/water-based nanofluids in a microchannel, with frequent change of heat flux and slip boundary condition, were studied by Nikkhah et al. [12]. Based on their results, local Nusselt number, along the length of the microchannel, changes periodically and enhances with the rising of Reynold's number. Furthermore, it was pointed out that an increase in the weight percentage of nanoparticles and slip coefficient results in the rise of Nusselt number, which is higher in upper Reynolds numbers.

The experimental investigation of forced convection of various nanofluids in a 500 μm width, 800 μm height, and 40 mm length microchannel was conducted by Nitiapiruk et al. [13]. Pure water and TiO_2-water with 0.5–2 vol.% were studied in this research. According to the outcomes of this research, the use of nanofluid with a volume fraction of 2 vol.% and minimum rate of heat flux and Reynold's number is more beneficial than other conditions.

An analytical approach was taken to study the entropy generation of alumina–water nanofluid inside circular microchannels and minichannels by Hassan et al. [14]. In their research, the Reynolds number was maintained constant at 1500, while the nanoparticle volume fraction and the diameter of channels differed from 0 to 0.14, and 3 mm (minichannel) to 0.05 mm (microchannel), respectively. They realized that water/Al_2O_3 nanofluid is an excellent coolant in minichannels under laminar flow regime. Nonetheless, employing high-viscous H_2O/Al_2O_3 nanofluid for laminar flow in microchannels is undesirable. Therefore, it is necessary to develop low-viscous Al_2O_3/water nanofluids in order to apply in microchannels under laminar flow condition.

Rimbault et al. [15] investigated convection heat transfer of nanofluids in a rectangular microchannel heat sink. The nanofluids were comprised of CuO nanoparticles combined with water as the base fluid in 0.24–4.5 volume fractions. The findings reveal that employment of copper oxide/water nanofluid for microchannel under the examined conditions does not offer great heat transfer improvement, compared to water. Such results were inconsistent with the experimental results reported by Zhang et al. [16] for alumina–water nanofluid flow through a circular microchannel, who indicated a significant increase in heat transfer rate and Nusselt number while using 0.25–0.75 vol.% nanofluid. While employing non-Newtonian Al_2O_3 nanofluid of up to 4% in a rectangular microchannel, the findings of Esmaeilnejad et al. [17] were consistent with those of Zhang et al. [16].

The literature survey reveals that combined use of nanofluids with microchannels gives higher heat transfer performance compared to the use of common, traditional fluids in conventional systems [18–20]. However, fulfilling the requirements from other applications of the microchannels needs additional advancement. A particular still uncomprehending case is the natural and mixed convection heat transfer of nanofluids in vertical and inclined ribbed microchannel heat sinks. In this work, dilute mixture of Cu nanoparticles and water has been analyzed in an inclined microchannel with four rectangular shaped ribs. Laminar mixed convection heat transfer was studied by the use of FLUENT software. Properties of nanofluids have been extracted from the available formulations in literature and introduced in the software. Model validation has been performed by the comparison of the simulation results and the existing literature. The focus was on the heat transfer of water-based nanofluids with variable volume fractions of solid nanoparticles in microchannels with different angles of

inclination. Results of this study may be applied in the use of coolants in various electronic devices such as high-power light-emitting diodes (LED), VLSI circuits, and micro-electro mechanical system (MEMS) [21].

2. Governing equations for laminar nanofluids

Dimensionless governing equations comprised of continuity, momentum, and energy equations, which are solved for laminar, steady-state flow in Cartesian coordinate system, are as follows [22, 23]:

$$\frac{\partial U}{\partial X}+\frac{\partial V}{\partial Y}=0 \tag{1}$$

$$U\frac{\partial U}{\partial X}+V\frac{\partial U}{\partial Y}=-\frac{\partial P}{\partial X}+\frac{\mu_{nf}}{\rho_{nf}\nu_{nf}}\frac{1}{\mathrm{Re}}\left(\frac{\partial^2 U}{\partial X^2}+\frac{\partial^2 U}{\partial Y^2}\right) \tag{2}$$

$$\mathrm{U}\frac{\partial V}{\partial X}+V\frac{\partial V}{\partial Y}=-\frac{\partial P}{\partial Y}+\frac{\mu_{nf}}{\rho_{nf}\upsilon_{nf}}\frac{1}{\mathrm{Re}}\left(\frac{\partial^2 V}{\partial X^2}+\frac{\partial^2 V}{\partial Y^2}\right)+\left(\frac{Gr}{\mathrm{Re}^2}\theta\right) \tag{3}$$

$$\mathrm{U}\frac{\partial \theta}{\partial X}+V\frac{\partial \theta}{\partial Y}=\frac{\alpha_{nf}}{\alpha_f}\frac{1}{\mathrm{Re}\,\mathrm{Pr}}\left(\frac{\partial^2 \theta}{\partial X^2}+\frac{\partial^2 \theta}{\partial Y^2}\right) \tag{4}$$

In the above equations, the following dimensionless parameters are used [24, 22]:

$$\begin{aligned}&\mathrm{X}=\frac{\mathrm{x}}{\mathrm{h}},\ \mathrm{Y}=\frac{\mathrm{y}}{\mathrm{h}},U=\frac{u}{u_{in}},V=\frac{v}{u_{in}},\mathrm{Pr}=\frac{\upsilon_f}{\alpha_f},\\&\theta=\frac{T-T_c}{T_h-T_c},\ \mathrm{Re}=\frac{u_{in}L_1}{\upsilon_f},\ \mathrm{P}=\frac{\overline{p}}{u_{in}^2\rho_{nf}},Gr=\frac{g\beta\left(T_h-T_c\right)L_1^3}{\upsilon^2}\end{aligned} \tag{5}$$

To calculate the local Nusselt number along the lower wall, the following relation is used [22]:

$$\mathrm{Nu(X)}=-\frac{k_{\mathrm{nf}}}{k_{\mathrm{f}}}\left(\frac{\partial\theta}{\partial Y}\right)_{Y=0} \tag{6}$$

The local Nusselt number across the ribs is given as

http://dx.doi.org/10.5772/62898

$$\mathrm{Nu(Y)} = -\frac{k_{\mathrm{nf}}}{k_{\mathrm{f}}}\left(\frac{\partial\theta}{\partial X}\right)_{X=0} \tag{7}$$

The local Nusselt number along each horizontal and vertical part of the lower wall can be expressed as follows:

$$\mathrm{Nu}_{\mathrm{m,x}} = \frac{l}{L_H}\int_0^{L_H} Nu(x)dx \tag{8}$$

$$\mathrm{Nu}_{\mathrm{m,y}} = \frac{l}{L_v}\int_0^{L_v} Nu(y)dy \tag{9}$$

Total **N**usselt number on the surface of each rib is calculated by

$$\mathrm{Nu}_{\mathrm{m,total}} = \mathrm{Nu}_{\mathrm{m,x}} + \mathrm{Nu}_{\mathrm{m,y}} \tag{10}$$

To calculate the local friction factor along the lower wall, the following relation is used:

$$C_f = \frac{\mu\dfrac{\partial u}{\partial y}}{0.5\rho u_{in}^2} \tag{11}$$

Substituting dimensionless parameters of Eq. (5) in Eq. (11), relation (12) and (13) are obtained as follows:

$$C_f(X) = \frac{2}{\mathrm{Re}}\left(\frac{\partial U}{\partial Y}\right)_{Y=0} \tag{12}$$

$$C_f(Y) = \frac{2}{\mathrm{Re}}\left(\frac{\partial V}{\partial X}\right)_{X=0} \tag{13}$$

The average friction factor along each horizontal part of the lower wall can be calculated as

$$C_{f_{\mathrm{m,x}}} = \frac{l}{L_H}\int_0^{L_H} C_f(x)dx \tag{14}$$

The average friction factor across each rib is defined as

$$C_{f_{\mathrm{m,y}}} = \frac{l}{L_v}\int_0^{L_y} C_f(y)dy \tag{15}$$

Total friction factor:

$$C_{f_{\mathrm{m,total}}} = C_{f_{\mathrm{m,x}}} + C_{f_{\mathrm{m,y}}} \tag{16}$$

2.1. Nanofluid properties

Table 1 shows the thermophysical properties of copper (as nanoparticles) and water (as base fluid). The thermophysical properties of the nanofluid can be acquired from the nanoparticles' characteristics as well as that of the base fluid.

	Copper (Cu)	**Water**
$\rho\left(\mathrm{Kg\ m^{-3}}\right)$	8933	997.1
$k\left(\mathrm{W\ m^{-1}\ K^{-1}}\right)$	400	0.613
$C_p\left(\mathrm{J\ Kg^{-1}\ K^{-1}}\right)$	385	4179
$\beta\left(\mathrm{K^{-1}}\right)$	0.0000167	0.00021
$\mu\left(\mathrm{Pa\ s}\right)$	–	0.000891

Table 1. Thermophysical properties of the base fluid and Cu nanoparticles [26].

Density and heat capacity of nanofluids can be computed through the recommended expressions by Goodarzi et al. [25], Togun et al. [26] and Safaei et al. [27]:

$$\rho_{nf} = \phi\rho_s + (1-\phi)\rho_f \tag{17}$$

$$\left(\rho c_p\right)_{nf} = (1-\phi)(\rho c_p)_f + \phi(\rho c_p)_s \tag{18}$$

For nanofluid thermal conductivity, Chon et al. [28] suggested a model for Al_2O_3–water which includes the influences of Brownian motion, viscous sublayer thickness, and temperature [29]:

http://dx.doi.org/10.5772/62898

$$\frac{k_{nf}}{k_f} = 1 + 64.7\phi^{0.746}\left(\frac{d_f}{d_s}\right)^{0.369}\left(\frac{k_s}{k_f}\right)^{0.7476} \mathrm{Pr}^{0.9955}\,\mathrm{Re}^{1.2321} \tag{19}$$

where $\mathrm{Re} = \frac{\rho_f k_b T}{3\pi\mu^2 l_f}$ and $\mathrm{Pr} = \frac{\mu_f}{\rho_f \alpha_f}$ are the Brownian Reynolds and Prandtl numbers, l_f is the mean free path of base fluid (0.17 nm for water), and μ is the temperature-dependent viscosity of the base fluid, represented as

$$\mu = Q \times 10^{\frac{O}{T-J}} \tag{20}$$

where *O, J*, and *Q* are constants. For water, they are equal to 247.8, 140, and 2.414×10^{-5}, respectively [29]. However, based on the previous studies by Karimipour et al. [30], the aforementioned correlation can be used with confidence for copper–water nanofluids.

Dynamic nanofluid viscosity is evaluated based on the recommendations of Brinkman [31]:

$$\mu_{nf} = \frac{\mu_f}{(1-\phi)^{2.5}} \tag{21}$$

The thermal expansion coefficient can be obtained from the suggested formula by Khanafer et al. [32] and Abouali and Ahmadi [33]:

$$\beta_{nf} = \beta_f \left[\frac{1}{1 + \frac{(1-\phi)\rho_f}{\phi\rho_s}} \frac{\beta_s}{\beta_f} + \frac{1}{1 + \frac{\phi\rho_s}{(1-\phi)\rho_f}} \right] \tag{22}$$

3. Boundary conditions

A 2-D microchannel with four same rectangular ribs was selected for the analysis. Investigation of heat transfer and fluid dynamics, including the study of velocity, thermal field, and friction effects, was performed in different angles of inclination. The schematic of the investigated microchannel is illustrated in **Figure 1**. The microchannel is 1350 μm long and 90 μm high. The length of the lower wall of the microchannel was divided into three parts. The temperature of 290.5 K was set at the inlet. The temperature of 305.5 K was considered in the middle part of the microchannel with the length of 450 μm, consisting of four ribs. The channel was insulated on the total length of the upper wall (L_1) as well as on the length of 450 μm of both left and right sides of the lower wall. Rectangular ribs in all the studied cases were considered to have a pitch, width, and height of 90, 15, and 30 μm (one-third of the microchannel's height),

respectively. In all cases, inclination angle between the microchannel and the horizon line was changed from 0° (horizontal case) to 90° (vertical case). A Reynolds number equal to 50 was selected to investigate the laminar flow, and Richardson number was varied between 0.1 and 10. Water as the base fluid was mixed with 0, 2, and 4% volume fractions of Cu nanoparticles (φ = 0.00, 0.02, and 0.04).

In this investigation, flow is considered to be incompressible, Newtonian, laminar, and single-phase. Thermophysical properties of nanofluid are assumed to remain unchanged with temperature.

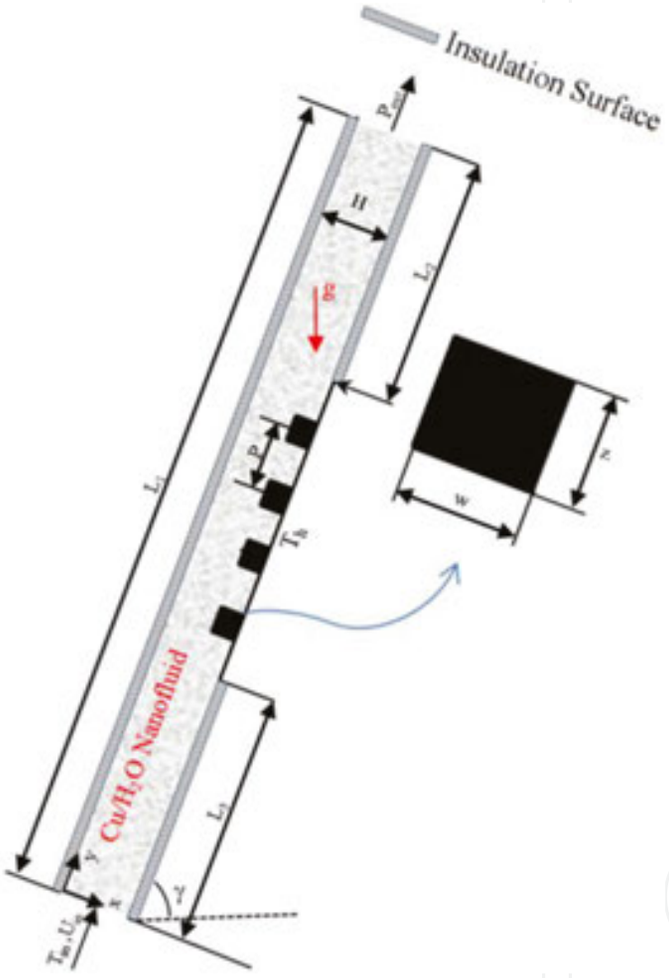

Figure 1. Schematic of the analyzed configuration.

4. Numerical method

The FLUENT commercial code was used to solve the partial differential equations that govern to the flow. The software applies the finite volume method, which is a particular case of the residual weighting method. This procedure is based on dividing the computational domain

http://dx.doi.org/10.5772/62898

into finite control volumes, each node of which surrounds with a control volume. The partial differential equation is afterward integrated over each finite volume [34].

The QUICK scheme [35] was applied for the discretization of all convective terms, while the SIMPLEC algorithm [36] was employed for pressure/velocity coupling. At one point, when the residuals for all equations fell under 10^{-7}, the calculation reached the convergence [37]. Heat transfer and fluid dynamics parameters can be assessed, after solving the governing equations.

5. Numerical procedure validation

5.1. Comparison with numerical and experimental study of water

Results of this study were compared with those of Salman et al. [38] for validation purposes. Validation has been performed with numerical and experimental data, considering fluid flow of water in a smooth microtube with Reynolds number equal to 90. **Figure 2** shows an excellent agreement between the simulation results of this work with both experimental and numerical results.

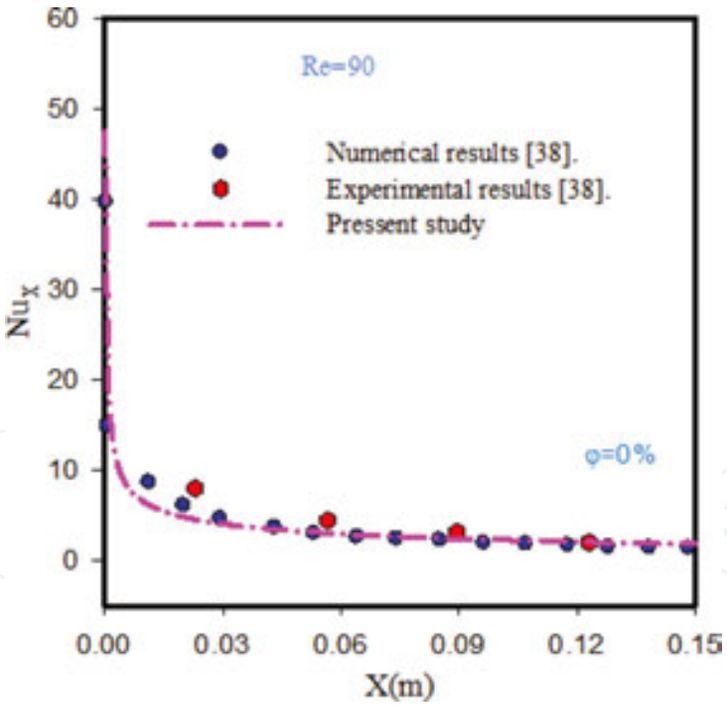

Figure 2. Local Nusselt number variation—comparison with the work of Salman et al. [38].

5.2. Comparison with numerical study of nanofluid

Aminossadati et al. [24] numerically investigated forced convection of water/Al_2O_3 in a horizontal microchannel. Middle part of the microchannel was exposed to a constant magnetic

field and heated by a constant heat flux. The effect of parameters such as Reynolds number, volume fraction of solid nanoparticles, and Hartmann number on the flow field and thermal performance of the microchannel was studied.

Figure 3 demonstrates excellent agreement between the present model's predictions and the numerical results of Aminossadati et al. [24] in different Reynolds numbers and volume fractions, in terms of average Nusselt number. This comparison shows that the present numerical method is reliable and is useful in predicting forced convection heat transfer inside a microchannel for nanofluids.

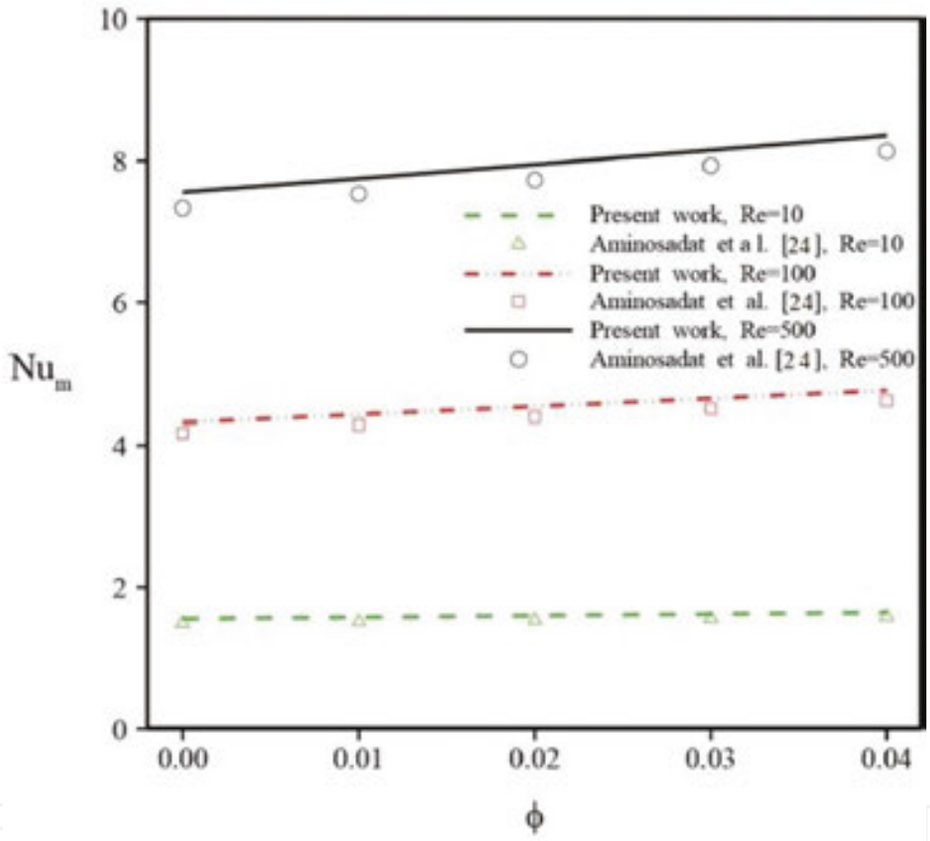

Figure 3. Averaged Nusselt number from present work versus that of Aminossadati et al. [24] for different values of Re and φ.

5.3. Grid independence

A structured, nonuniform grid has been chosen for the discretization of the computational domain. A more refined grid was applied near the walls, where temperature and velocity gradients are sensitive. Grid independency of the computational domain was tested by using various grid distributions. Average Nusselt number and dimensionless pressure drop for each number of grids are shown in **Figure 4(A, B)** , from which a grid of 60 × 900 was chosen for all the simulation cases.

http://dx.doi.org/10.5772/62898

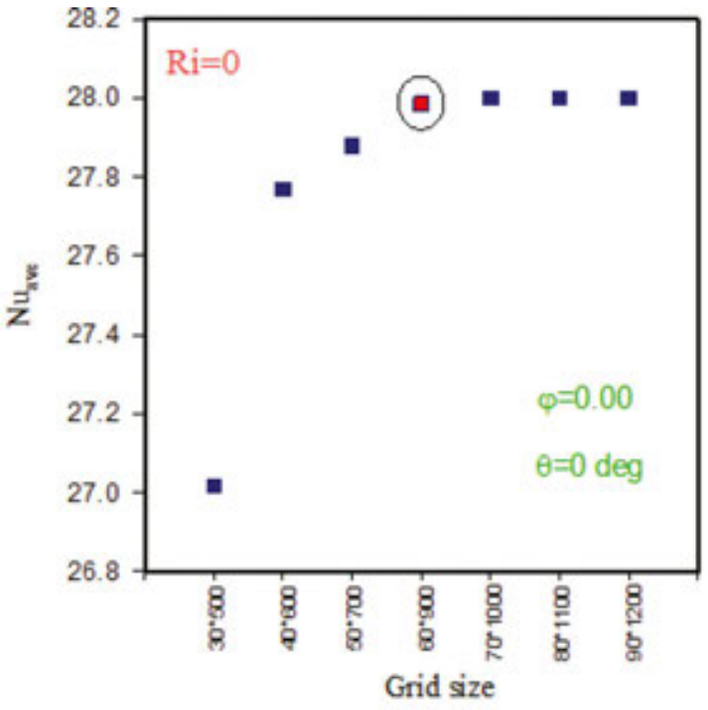

(A) Average Nusselt number

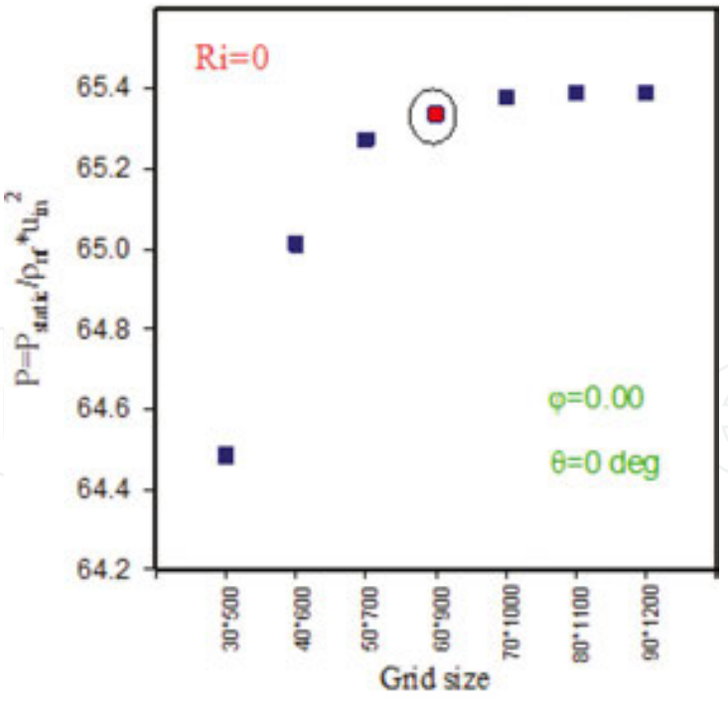

(B) Pressure drop

Figure 4. Grid independence tests for the present study by comparison of average Nusselt number and dimensionless pressure drop in various mesh concentrations: (A) average Nusselt number and (B) pressure drop.

6. Results and discussion

Inside an inclined microchannel with four rectangular ribs, mixed convection heat transfer of water–coppernanofluid is studied, utilizing finite volume method (**Figure 1**). The distances between the ribs and their lengths and widths are supposed to be constant. The simulation results are plotted in the form of contours and diagrams.

The isotherm contours and streamlines for $\gamma = 90°$, Re = 50, different Richardson numbers, and volume fraction of 4% are shown in **Figure 5 (A, B)**. After the microchannel's entry, the flow attains a fully developed hydrodynamic regime. When the fluid reaches the ribs, its direction is diverted and will result in an increased vertical component of the velocity. Yet, increased Richardson number does not lead to any change in the streamlines' variations. In case of isotherms' illustrations along the microchannel, once fluid with temperature of T_h arrives in the rib-roughened areas with T_c(surface temperature), temperature of fluid decreases, and heat is transferred between the rib-roughened surfaces and fluid. Along the microchannel, ribs function as a mixer and reduce the temperature gradient between the surface and the fluid, and afterwards, the rate of heat transfer increases. These variations in heat transfer improve as the inclination angle (γ) or Richardson number increases. The first influential factor is the resultant from the gravity and variations in its components—perpendicular to and in line with the flow fluid—along the microchannel. Once γ increases from 0 to 90°, the terms of diffusion and advection in natural convection heat transfer strengthen, which leads to isothermal line variations.

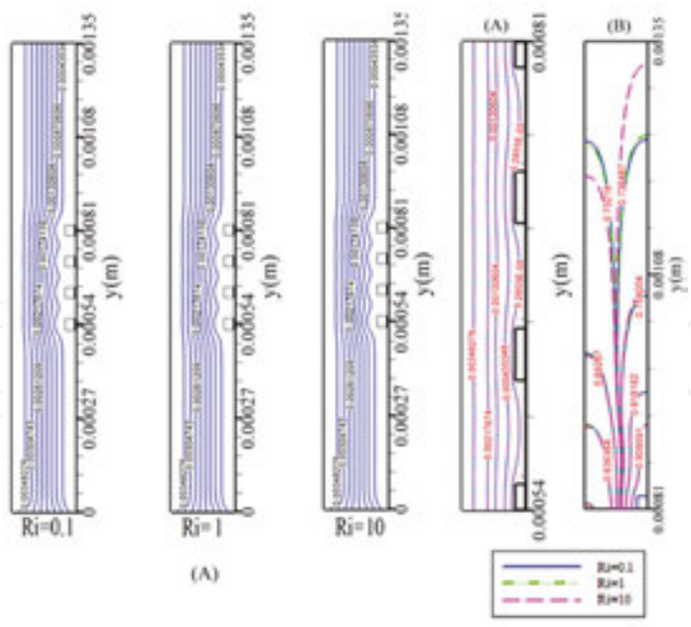

Figure 5. (A) Streamlines and (B) Isotherm contours for 4% volume fraction and $\gamma = 90°$.

The dimensionless velocity contours for Ri = 10, 2% volume fraction, and 30°, 45°, 60°, and 90° inclination angles, in line with (A) and perpendicular (B) to the flow are demonstrated in **Figure**

http://dx.doi.org/10.5772/62898

6 (A, B). The increasing γ exerts a significant effect on fluid flow behavior and heat transfer. The velocity components (perpendicular to and along with the flow) vary by flowing the fluid along the microchannel, because of the ribs. Increased inclination angle intensifies these variations. The outcomes showed that the perpendicular velocity component exhibited more variation, which causes vortexes and reverse flows in the flow field. Consequently, this velocity component is deemed more effective, because its intensification can improve flow mixing and rate of heat transfer.

Figure 6. Dimensionless velocity contours for 2% volume fraction, different inclination angles, and Ri = 10: (A) along the flow and (B) perpendicular to the flow.

The average Nusselt number for a ribbed microchannel with various volume fractions, different Ri, and inclination angles is depicted in **Figure 7**. The results endorse that the average

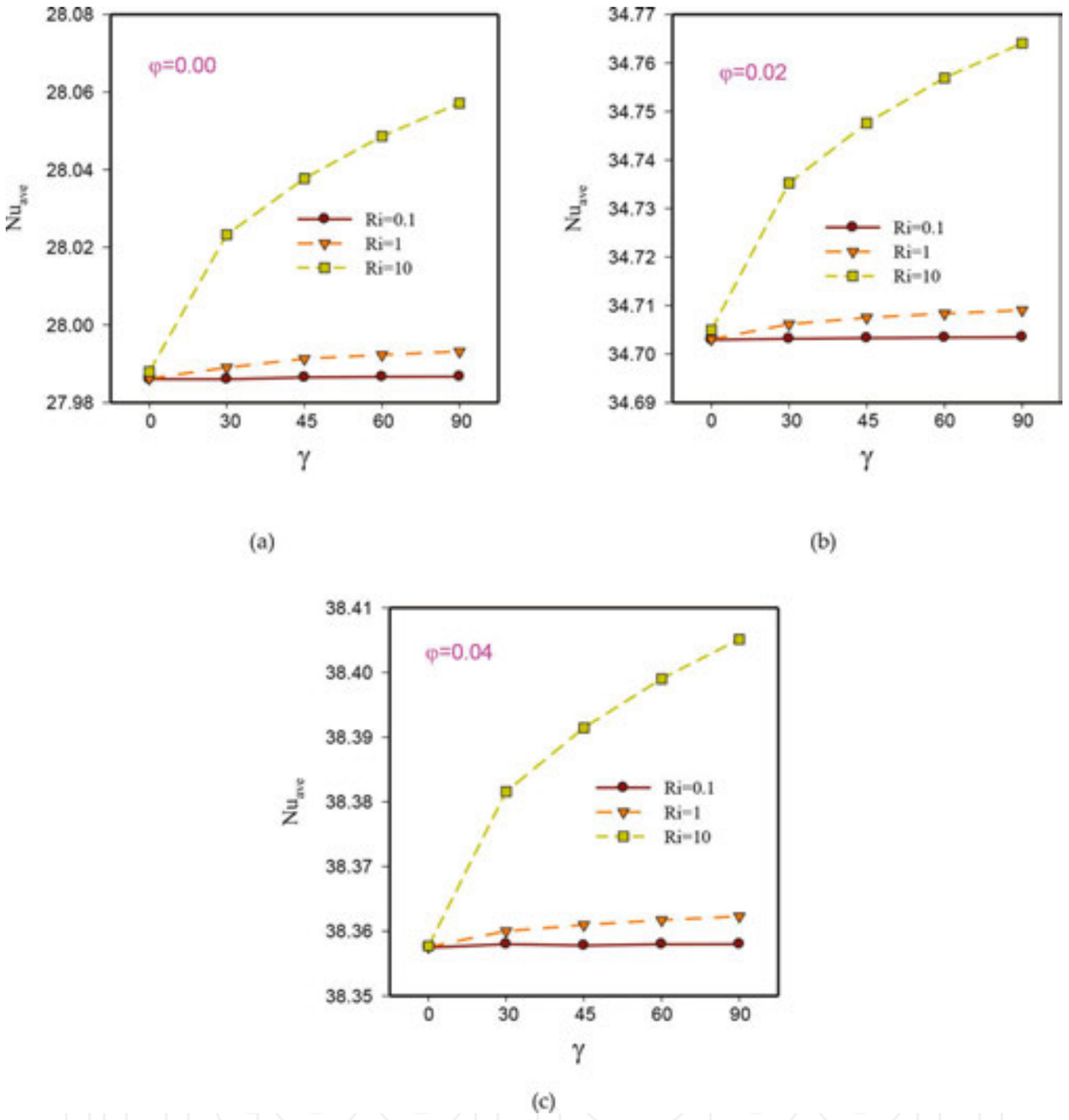

Figure 7. Profiles of average Nusselt number for different Richardson numbers and volume fractions of nanoparticles.

Nusselt number increased by increasing the Richardson number, inclination angle, and nanofluid volume fraction. Nevertheless, a significant increase in the average Nusselt number is seen compared to others for Ri = 10. Also, in all volume fractions, the average Nusselt number is higher when Ri = 1 compared with Ri = 0.1. This can be attributed to the fact that as the Richardson number increases, the effective terms in natural convection heat transfer are strengthened. Moreover, increased volume fraction of nanoparticles significantly affects fluids' thermal conductivity, which enhances the rate of nanofluid heat transfer. Even though

http://dx.doi.org/10.5772/62898

when Ri = 0.1, the increment of average Nusselt number is nearly independent of γ, the heat transfer is increased with an increase in γ in higher Richardson numbers. The reason can be the velocity component variations, which rise mixing of the fluid layers.

The local Nusselt number for the distillated water and nanofluids on the lower wall of the microchannel, γ = 90°, and different Richardson numbers is compared in **Figure 8**. As can be seen, nanofluid has a greater Nusselt number than the distillated water, because of the existence of nanoparticles with greater thermal conductivity and also the effect of Brownian motion on the nanofluid's thermal conductivity. Other factors that increase the Nusselt number are the ribs, which lead to abrupt upsurge of the heat transfer rate in the rib-roughened parts. It is primarily due to improved mixing of the fluid layers between cold fluid and hot area. Thermal boundary layer is altered and reformed when the fluid hits the ribs, which eventually increases the rate of heat transfer.

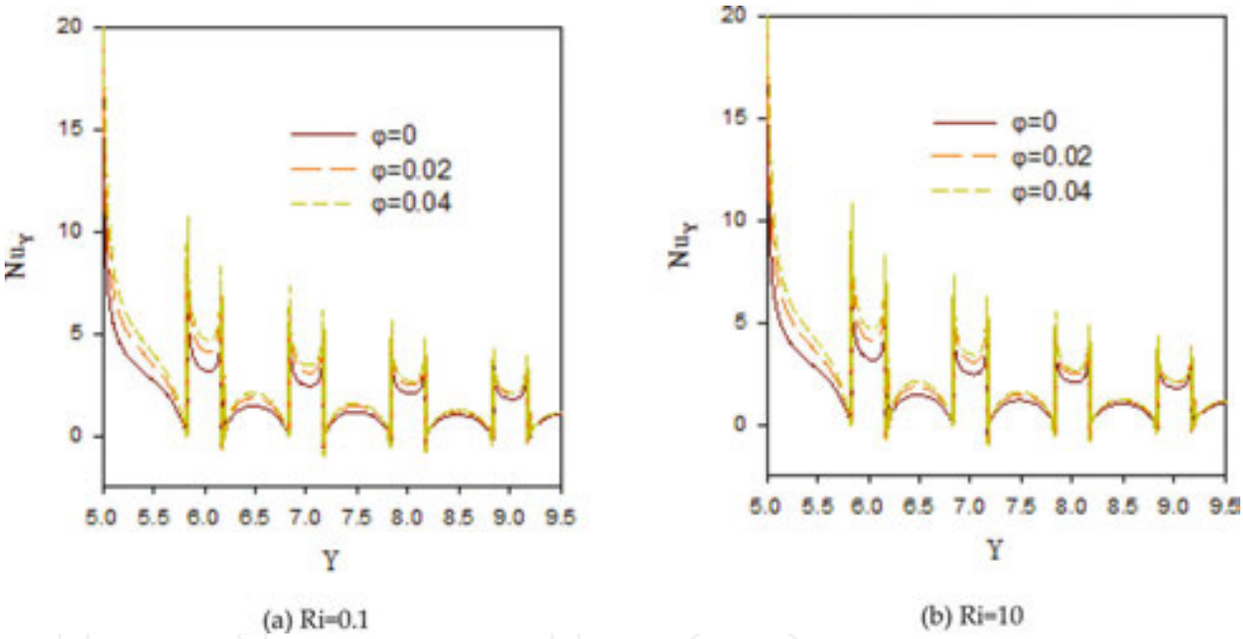

Figure 8. Local Nusselt number on lower rib-roughened wall for γ = 90°: (A) Ri = 0.1; (B) Ri = 10.

The pressure drop values for different Richardson numbers and volume fractions are shown in **Figure 9**. It was observed that in all studied cases, pressure drop augments as the volume fractions of nanoparticles, Richardson number, or inclination angle increase. In the cooling fluid, solid nanoparticles cause a significant drop in pressure owing to the flow of denser, high-viscous fluid, compared with the fluid with lower density and viscosity. More vortexes are created as a result of increased inclination angle of the microchannel and the flow is reversed, which necessitate more energy to increase the pressure drop. Likewise, the pressure drop increases by transition from forced convection domination to free convection one, as a result of high variations of gravity components in higher Richardson numbers.

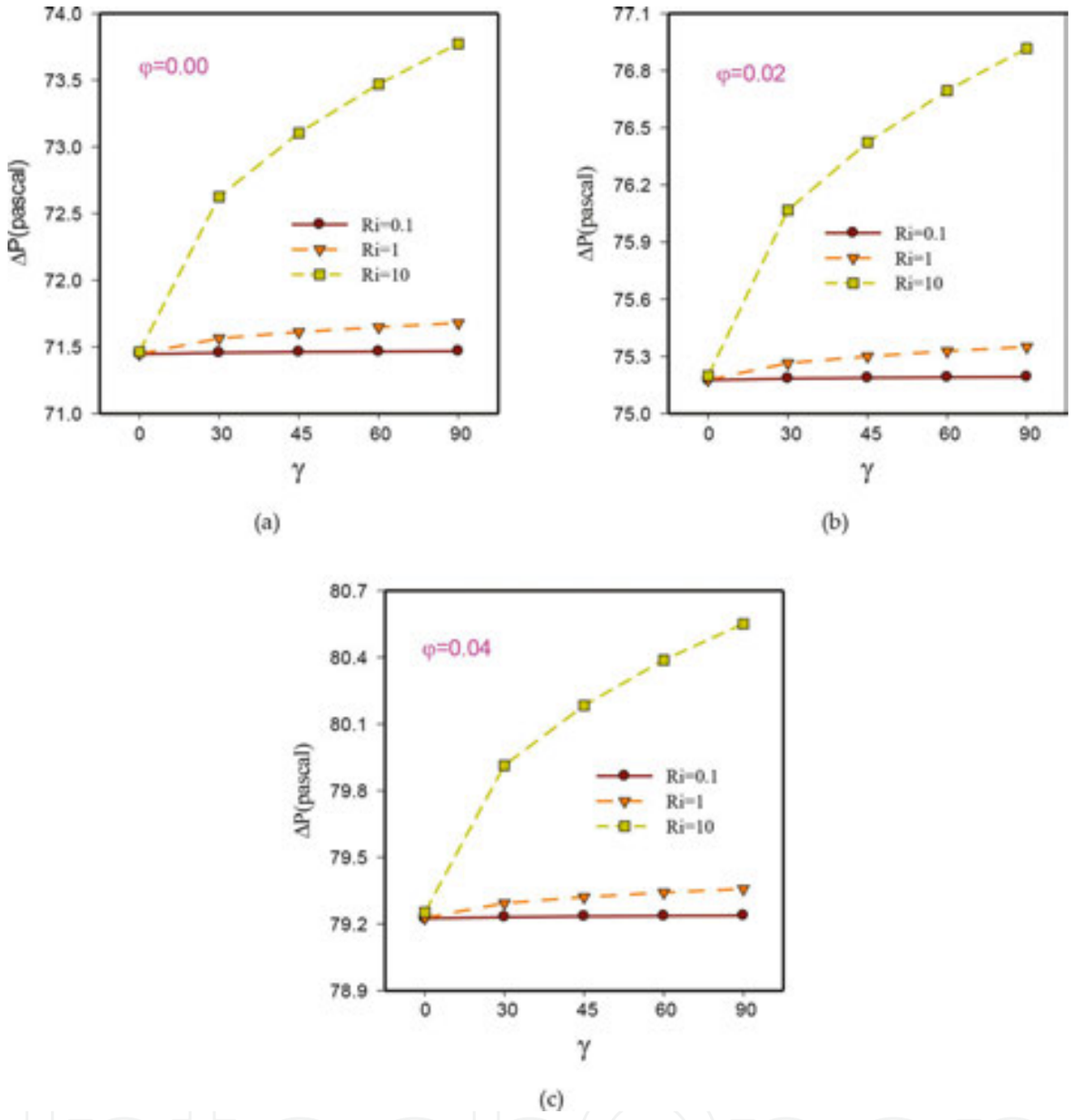

Figure 9. Pressure drop diagram for different Richardson numbers and volume fractions of nanoparticles.

The average friction factor for different Richardson numbers and volume fractions on the upper wall of the microchannel are shown in **Figure 10**. The average friction factor drops as the nanoparticle volume fraction decreases, and Richardson number and inclination angle increase. The density and dynamic viscosity of the fluid are intensified as the nanoparticle volume fraction increases, which leads to an increment in the average friction factor. Also, collision of particles with the microchannel's surface increases in higher nanoparticle volume fraction, which raises the friction factor. The friction factor is more or less independent from γ for the case of forced convection domination. Nevertheless, with an increase in inclination angle or Richardson number, the friction factor on the upper wall drops because of gradient reduction in axial velocity in line with the upper wall of the microchannel.

http://dx.doi.org/10.5772/62898

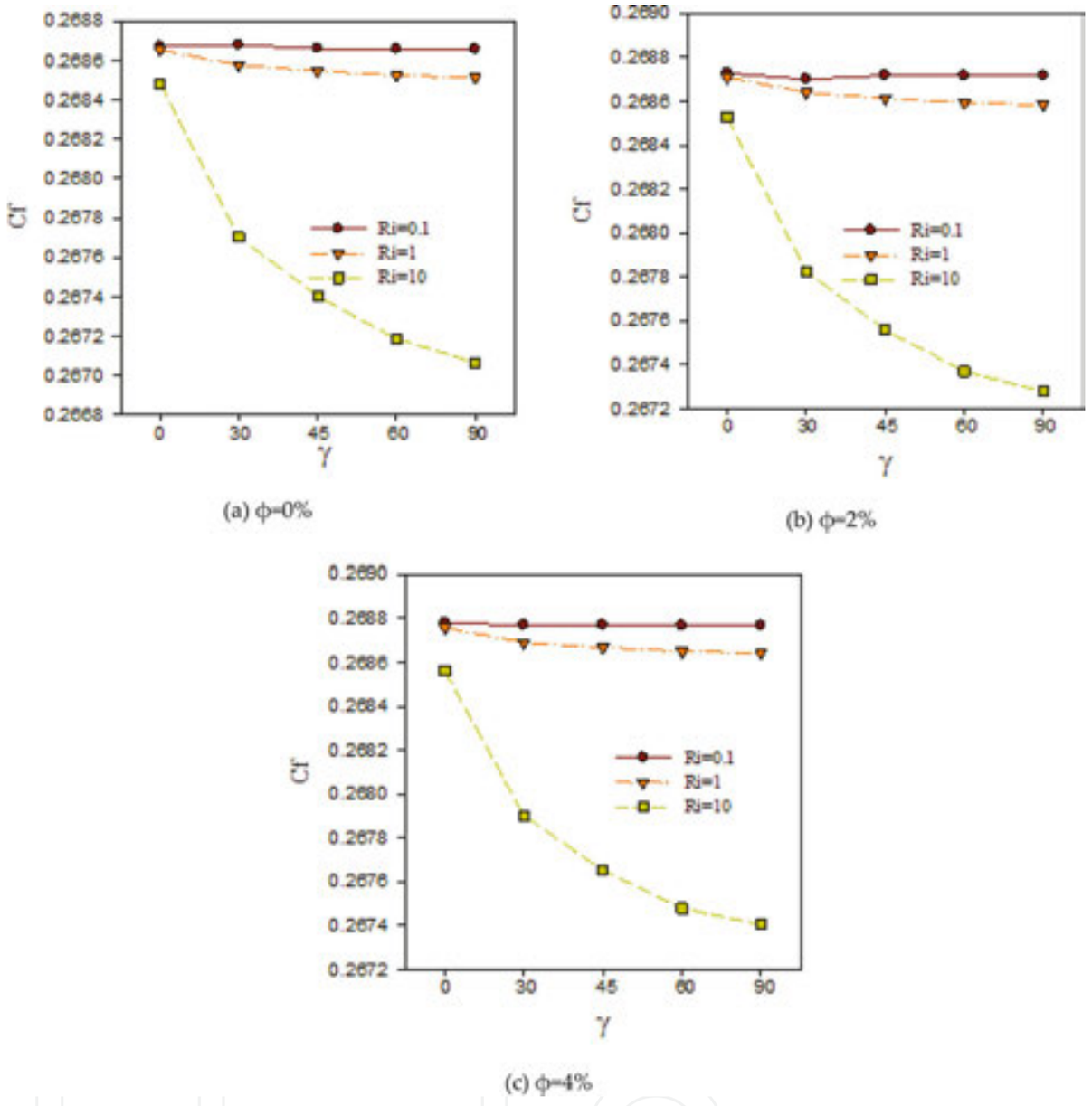

Figure 10. Average friction factor on microchannel's top wall. (A) φ=0%; (B) φ=2%; (C) φ=4%.

The dimensionless temperature profiles in different inclination angles and microchannel cross sections for $\varphi = 0.04$ and Ri = 1 are demonstrated in **Figure 11**. It can be seen that approaching microchannel's outlet cross section or increasing inclination angle of microchannel decreases the dimensionless temperature of hot fluid for all cases. This results in better mixing of fluid layers, and lastly, increase of heat transfer.

Higher inclination angles result in development of intensive vortexes and better fluid mixing, which significantly decrease the dimensionless temperature, particularly in near-inlet cross sections. Thus, the dimensionless temperature for the vertical microchannel has the least value in all cross sections, meaning that this microchannel angle has the maximum rate of heat transfer.

At sections near to the entry, the dimensionless temperature profile drops, because the thermal boundary layer has not been developed yet. The thermal boundary layer becomes fully developed as the entry length is increased, which increases the dimensionless temperature.

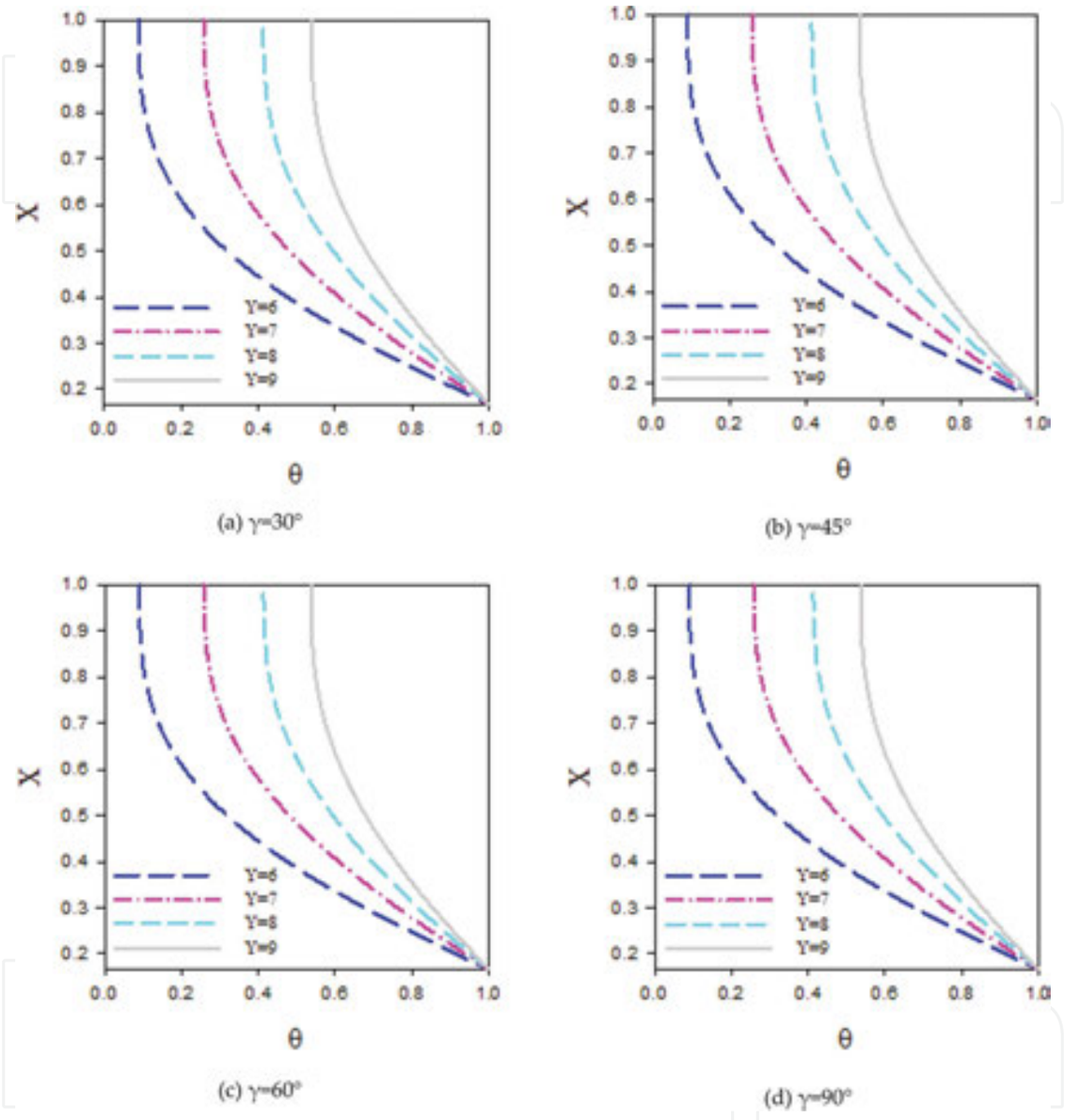

Figure 11. Profiles of dimensionless temperature in different microchannel cross sections for Ri = 1 and φ = 0.04. (A) γ=30°; (B) γ=45°; (C) γ=60°; (D) γ=90°.

7. Conclusions

In this work, the fluid flow and heat transfer of laminar Cu–water nanofluid in a 2D rectangular ribbed microchannel with different inclination angles and Richardson numbers were investigated. Simulation of the problem was performed by the use of finite volume method. Reynolds

http://dx.doi.org/10.5772/62898

number of 50 and Richardson numbers between 0.1 and 10 were applied to the simulation. Solid nanoparticles were chosen to have a volume fraction of 0.0–4.0%.

The results of this research revealed that increasing the inclination angle of microchannel or volume fraction of solid particles enhances the heat transfer rate. Existence of ribs through the flow path results in velocity gradient and increases the fluid contact with the surfaces of the microchannel, which in turn enhances heat transfer, while increasing the average friction factor. Addition of nanoparticles to the base fluid does not majorly affect the hydrodynamic parameters of the flow such as fluid velocity. Of all the studied cases, maximum heat transfer can be seen in a vertical microchannel, dominated by natural convection, because of the significant effect of gravity on the fluid structure and enhanced mixing of the fluid layers; and the lowest Nusselt number belongs to the horizontal microchannel dominated by forced convection.

Acknowledgements

The authors gratefully acknowledge High Impact Research Grant UM.C/HIR/MOHE/ENG/23 and Faculty of Engineering, University of Malaya, Malaysia for support in conducting this research work.

Nomenclature

x, y	Cartesian coordinates (m)
D	Diameter (m)
X, Y	Dimensionless coordinates
U, V	Dimensionless flow velocity in x–y direction
H, L	Dimensionless microchannel height and length
P	Fluid pressure (Pa)
C_f	Friction factor
Gr	Grashof number
G	Gravity acceleration (m/s^2)
C_p	Heat capacity (J/kg K)
u_{in}	Inlet flow velocity (m/s)
h, l	Microchannel height and length (m)
Nu	Nusselt number
Pr	Prandtl number
Re	Reynolds number
T	Temperature, K

K	Thermal conductivity, W/m K
u, v	velocity components in x, y directions, m/s

Greek symbols

κ_b	Boltzmann constant (J/K)
ρ	Density (kg/m^3)
θ	Dimensionless temperature
μ	Dynamic viscosity (Pa s)
υ	Kinematics viscosity (m^2/s)
φ	Nanoparticles volume fraction
Γ	The angle between ribs and horizon line (°)
α	Thermal diffusivity (m^2/s)
β	Thermal expansion coefficient (1/ K)

Superscripts and subscripts

F	Base fluid (distillated water)
C	Cold
H	Hot
H	Horizontal
In	Inlet
M	Mean
Nf	Nanofluid
S	Solid nanoparticles
total	Total
V	Vertical

Author details

Mohammad Reza Safaei[1*], Marjan Gooarzi[2], Omid Ali Akbari[3,4], Mostafa Safdari Shadloo[5] and Mahidzal Dahari[6]

*Address all correspondence to: cfd_safaei@um.edu.my; cfd_safaei@yahoo.com

1 Department of Mechanical Engineering, Faculty of Engineering, University of Malaya, Kuala Lumpur, Malaysia

2 Young Researchers and Elite Club, Mashhad Branch, Islamic Azad University, Mashhad, Iran

3 Department of Mechanical Engineering, Aligoudarz Branch, Islamic Azad University, Aligoudarz, Iran

4 Department of Mechanical Engineering, Azna Branch, Islamic Azad University, Azna, Iran

5 CORIA-UMR 6614, Normandie University, CNRS-University & INSA of Rouen, Rouvray, France

6 Department of Electrical Engineering, Faculty of Engineering, University of Malaya, Kuala Lumpur, Malaysia

References

[1] Sakanova A, Keian CC, Zhao J. Performance improvements of microchannel heat sink using wavy channel and nanofluids. International Journal of Heat and Mass Transfer. 2015;89:59–74. doi:http://dx.doi.org/10.1016/j.ijheatmasstransfer.2015.05.033.

[2] Tuckerman DB, Pease R. High-performance heat sinking for VLSI. Electron Device Letters, IEEE. 1981;2(5):126–129.

[3] Sohel M, Saidur R, Sabri MFM, Kamalisarvestani M, Elias M, Ijam A. Investigating the heat transfer performance and thermophysical properties of nanofluids in a circular micro-channel. International Communications in Heat and Mass Transfer. 2013;42:75–81.

[4] Nimmagadda R, Venkatasubbaiah K. Conjugate heat transfer analysis of micro-channel using novel hybrid nanofluids (Al_2O_3+Ag/water). European Journal of Mechanics - B/Fluids. 2015;52:19–27. doi:http://dx.doi.org/10.1016/j.euromechflu.2015.01.007.

[5] Khaled ARA, Vafai K. Cooling augmentation using microchannels with rotatable separating plates. International Journal of Heat and Mass Transfer. 2011;54(15–16):3732–3739. doi:http://dx.doi.org/10.1016/j.ijheatmasstransfer.2011.02.054.

[6] Vafai K, Khaled ARA. Analysis of flexible microchannel heat sink systems. International Journal of Heat and Mass Transfer. 2005;48(9):1739–1746. doi:http://dx.doi.org/10.1016/j.ijheatmasstransfer.2004.11.020.

[7] Goodarzi M, Amiri A, Goodarzi MS, Safaei MR, Karimipour A, Languri EM et al. Investigation of heat transfer and pressure drop of a counter flow corrugated plate heat

exchanger using MWCNT based nanofluids. International Communications in Heat and Mass Transfer. 2015;66:172–179.

[8] Sarafraz MM, Hormozi F. Experimental study on the thermal performance and efficiency of a copper made thermosyphon heat pipe charged with alumina–glycol based nanofluids. Powder Technology. 2014;266:378–387. doi:http://dx.doi.org/10.1016/j.powtec.2014.06.053.

[9] Goshayeshi HR, Goodarzi M, Safaei MR, Dahari M. Experimental study on the effect of inclination angle on heat transfer enhancement of a ferrofluid in a closed loop oscillating heat pipe under magnetic field. Experimental Thermal and Fluid Science. 2016;74:265–270. doi:http://dx.doi.org/10.1016/j.expthermflusci.2016.01.003.

[10] Kalteh M, Abbassi A, Saffar-Avval M, Frijns A, Darhuber A, Harting J. Experimental and numerical investigation of nanofluid forced convection inside a wide microchannel heat sink. Applied Thermal Engineering. 2012;36:260–268. doi:http://dx.doi.org/10.1016/j.applthermaleng.2011.10.023.

[11] Malvandi A, Ganji DD. Brownian motion and thermophoresis effects on slip flow of alumina/water nanofluid inside a circular microchannel in the presence of a magnetic field. International Journal of Thermal Sciences. 2014;84:196–206. doi:http://dx.doi.org/10.1016/j.ijthermalsci.2014.05.013.

[12] Nikkhah Z, Karimipour A, Safaei MR, Forghani-Tehrani P, Goodarzi M, Dahari M et al. Forced convective heat transfer of water/functionalized multi-walled carbon nanotube nanofluids in a microchannel with oscillating heat flux and slip boundary condition. International Communications in Heat and Mass Transfer. 2015;68:69–77.

[13] Nitiapiruk P, Mahian O, Dalkilic AS, Wongwises S. Performance characteristics of a microchannel heat sink using TiO_2/water nanofluid and different thermophysical models. International Communications in Heat and Mass Transfer. 2013;47:98–104. doi:http://dx.doi.org/10.1016/j.icheatmasstransfer.2013.07.001.

[14] Hassan M, Sadri R, Ahmadi G, Dahari MB, Kazi SN, Safaei MR et al. Numerical study of entropy generation in a flowing nanofluid used in micro-and minichannels. Entropy. 2013;15(1):144–155.

[15] Rimbault B, Nguyen CT, Galanis N. Experimental investigation of CuO–water nanofluid flow and heat transfer inside a microchannel heat sink. International Journal of Thermal Sciences. 2014;84:275–292. doi:http://dx.doi.org/10.1016/j.ijthermalsci.2014.05.025.

[16] Zhang H, Shao S, Xu H, Tian C. Heat transfer and flow features of Al_2O_3–water nanofluids flowing through a circular microchannel—Experimental results and correlations. Applied Thermal Engineering. 2013;61(2):86–92. doi:http://dx.doi.org/10.1016/j.applthermaleng.2013.07.026.

[17] Esmaeilnejad A, Aminfar H, Neistanak MS. Numerical investigation of forced convection heat transfer through microchannels with non-Newtonian nanofluids. Interna-

tional Journal of Thermal Sciences. 2014;75:76–86. doi:http://dx.doi.org/10.1016/j.ijthermalsci.2013.07.020.

[18] Karimipour A, Hossein Nezhad A, D'Orazio A, Hemmat Esfe M, Safaei MR, Shirani E. Simulation of copper–water nanofluid in a microchannel in slip flow regime using the lattice Boltzmann method. European Journal of Mechanics - B/Fluids. 2015;49, Part A: 89–99. doi:http://dx.doi.org/10.1016/j.euromechflu.2014.08.004.

[19] Hedayati F, Malvandi A, Kaffash MH, Ganji DD. Fully developed forced convection of alumina/water nanofluid inside microchannels with asymmetric heating. Powder Technology. 2015;269:520–531. doi:http://dx.doi.org/10.1016/j.powtec.2014.09.034.

[20] Salman BH, Mohammed HA, Munisamy KM, Kherbeet AS. Characteristics of heat transfer and fluid flow in microtube and microchannel using conventional fluids and nanofluids: a review. Renewable and Sustainable Energy Reviews. 2013;28:848–880. doi:http://dx.doi.org/10.1016/j.rser.2013.08.012.

[21] Hadadian M, Samiee S, Ahmadzadeh H, Goharshadi EK. Nanofluids for heat transfer enhancement—A review. Physical Chemistry Research. 2013;1(1):1–33.

[22] Raisi A, Ghasemi B, Aminossadati S. A numerical study on the forced convection of laminar nanofluid in a microchannel with both slip and no-slip conditions. Numerical Heat Transfer, Part A: Applications. 2011;59(2):114–129.

[23] Sharif M. Laminar mixed convection in shallow inclined driven cavities with hot moving lid on top and cooled from bottom. Applied Thermal Engineering. 2007;27(5): 1036–1042.

[24] Aminossadati S, Raisi A, Ghasemi B. Effects of magnetic field on nanofluid forced convection in a partially heated microchannel. International Journal of Non-Linear Mechanics. 2011;46(10):1373–1382.

[25] Goodarzi M, Safaei MR, Vafai K, Ahmadi G, Dahari M, Kazi SN et al. Investigation of nanofluid mixed convection in a shallow cavity using a two-phase mixture model. International Journal of Thermal Sciences. 2014;75:204–220. doi:http://dx.doi.org/10.1016/j.ijthermalsci.2013.08.003.

[26] Togun H, Ahmadi G, Abdulrazzaq T, Shkarah AJ, Kazi S, Badarudin A et al. Thermal performance of nanofluid in ducts with double forward-facing steps. Journal of the Taiwan Institute of Chemical Engineers. 2015;47:28–42.

[27] Safaei MR, Togun H, Vafai K, Kazi S, Badarudin A. Investigation of heat transfer enhancement in a forward-facing contracting channel using FMWCNT nanofluids. Numerical Heat Transfer, Part A: Applications. 2014;66(12):1321–1340.

[28] Chon CH, Kihm KD, Lee SP, Choi SUS. Empirical correlation finding the role of temperature and particle size for nanofluid (Al_2O_3) thermal conductivity enhancement. Applied Physics Letters. 2005;87(15):153107—153107-3.

[29] Mintsa HA, Roy G, Nguyen CT, Doucet D. New temperature dependent thermal conductivity data for water-based nanofluids. International Journal of Thermal Sciences. 2009;48(2):363–371.

[30] Karimipour A, Nezhad A, Behzadmehr A, Alikhani S, Abedini E. Periodic mixed convection of a nanofluid in a cavity with top lid sinusoidal motion. Proceedings of the Institution of Mechanical Engineers, Part C: Journal of Mechanical Engineering Science. 2011;225:2149–2160.

[31] Brinkman H. The viscosity of concentrated suspensions and solutions. The Journal of Chemical Physics. 1952;20(4):571–.

[32] Khanafer, Vafai K, Lightstone M. Buoyancy-driven heat transfer enhancement in a two-dimensional enclosure utilizing nanofluids. International Journal of Heat and Mass Transfer. 2003;46(19):3639–3653.

[33] Abouali O, Ahmadi G. Computer simulations of natural convection of single phase nanofluids in simple enclosures: a critical review. Applied Thermal Engineering. 2012;36:1–13.

[34] Patankar SV. Numerical Heat Transfer and Fluid Flow, Series in Computational Methods in Mechanics and Thermal Sciences. Hemisphere Publishing Corporation; 1980.

[35] Rahmanian B, Safaei MR, Kazi SN, Ahmadi G, Oztop HF, Vafai K. Investigation of pollutant reduction by simulation of turbulent non-premixed pulverized coal combustion. Applied Thermal Engineering. 2014;73(1):1222–1235.

[36] Goodarzi M, Safaei M, Karimipour A, Hooman K, Dahari M, Kazi S et al. Comparison of the finite volume and lattice Boltzmann methods for solving natural convection heat transfer problems inside cavities and enclosures. Abstract and Applied Analysis. 2014;2014(Article ID 762184):1–15. doi:10.1155/2014/762184.

[37] Goodarzi M, Safaei M, Oztop HF, Karimipour A, Sadeghinezhad E, Dahari M et al. Numerical study of entropy generation due to coupled laminar and turbulent mixed convection and thermal radiation in an enclosure filled with a semitransparent medium. The Scientific World Journal. 2014;2014:1–8.

[38] Salman B, Mohammed H, Kherbeet AS. Numerical and experimental investigation of heat transfer enhancement in a microtube using nanofluids. International Communications in Heat and Mass Transfer. 2014;59:88–100.